minerals

MDPI

Article

Reduced Graphene Oxide Membranes as Potential Self-Assembling Filter for Wastewater Treatment

Saverio Latorrata [1,*], Cinzia Cristiani [1], Andrea Basso Peressut [1,*], Luigi Brambilla [1], Maurizio Bellotto [1], Giovanni Dotelli [1], Elisabetta Finocchio [2], Paola Gallo Stampino [1] and Gianguido Ramis [2]

[1] Dipartimento di Chimica, Materiali e Ingegneria Chimica "Giulio Natta", Politecnico di Milano, Piazza Leonardo Da Vinci 32, 20133 Milano, Italy; cinzia.cristiani@polimi.it (C.C.); luigi.brambilla@polimi.it (L.B.); mauriziopietro.bellotto@polimi.it (M.B.); giovanni.dotelli@polimi.it (G.D.); paola.gallo@polimi.it (P.G.S.)

[2] Dipartimento di Ingegneria Civile, Chimica e Ambientale, Università di Genova, Via all'Opera Pia 15, 16145 Genova, Italy; elisabetta.finocchio@unige.it (E.F.); gianguidoramis@unige.it (G.R.)

* Correspondence: saverio.latorrata@polimi.it (S.L.); andreastefano.basso@polimi.it (A.B.P.); Tel.: +39-02-2399-3190 (S.L.); +39-02-2399-3231 (A.B.P.)

Abstract: This work focuses on the investigation of the capability of reduced graphene oxide (rGO) filters to remove metals from various wastewater. The process to produce rGO membranes is reported and discussed, as well as their ability to capture ions in complex solutions, such as tap or industrial wastewater. Multi-ion solutions, containing Cu^{2+}, Fe^{3+}, Ni^{2+}, and Mn^{2+} to simulate mine wastewater, or Ca^{2+} and Mg^{2+} to mimic drinkable water, were used as models. In mono-ionic solutions, the best capture efficiency values were proved for Ca^{2+}, Fe^{3+}, and Ni^{2+} ions, while a matrix effect was found for multi-ion solutions. However, interesting capture efficiencies were measured in the range of 30–90%, depending on the specific ion, for both single and multi-ion solutions. An attempt is proposed to correlate ions capture efficiency with ions characteristics, such as ionic radius or charge. Combining a satisfactory capture efficiency with low costs and ease of treatment unit operations, the approach here proposed is considered promising to replace other more complex and expensive filtration techniques.

Keywords: wastewater treatment; heavy metals; filtration; graphene oxide; self-assembling membranes

Citation: Latorrata, S.; Cristiani, C.; Basso Peressut, A.; Brambilla, L.; Bellotto, M.; Dotelli, G.; Finocchio, E.; Gallo Stampino, P.; Ramis, G. Reduced Graphene Oxide Membranes as Potential Self-Assembling Filter for Wastewater Treatment. *Minerals* **2021**, *11*, 15. https://dx.doi.org/10.3390/min11010015

Received: 7 November 2020
Accepted: 23 December 2020
Published: 25 December 2020

1. Introduction

In recent years, recovery and reuse of freshwater resources has represented one of the technological and social challenges to be faced in order to improve the quality of human life. The use of water impacts on many aspects of civil, industrial, and agricultural applications [1,2]. Among others, causes of pollution are found in the use of pesticides, fertilizers, heavy metals and in plastic materials.

From a theoretical point of view, a purification treatment can be developed for any type of wastewater, but a strong limitation is given by the possibility to achieve effective and economical solutions [2,3]. The selection of the most appropriate treatment depends on several factors: removal of the contaminants, reliability and flexibility of the technology, costs, environmental compatibility, process scalability [4]. Available technologies can be grouped in two classes: liquid-liquid systems, based on selective extractions with organic solvents, and solid-liquid systems that mainly use ion exchange resins or solid adsorbents as filters. The adsorption/filtration process is performed in a column, a tube, or in a cartridge containing the adsorbent material. Following the adsorption step, the filter and the ions retained therein can be disposed of or, more desirably, the filter can be recycled and the adsorbed species recovered [5,6]. A number of sorbent solids are usually employed, such as activated carbon, silica gel, pristine, and modified clay, activated silico-aluminates and polymeric materials [7,8].

Recently, innovative systems based on carbon nanotubes, nanofibers, graphene, and graphene oxide have been proposed in the scientific literature, aiming to improve the purification ability with reduced amount of sorbent material [9–11]. Although the effectiveness of such novel carbon-based materials is well-known and demonstrated, their use still presents open problems. For instance, the precursors that are needed to produce the sorbents can contain variable amounts of both organic and inorganic impurities, which might contaminate the water as well [5,9]. Moreover, sorbents selectivity still represents an issue to be solved.

Therefore, several research groups have proposed the modification and the functionalization of carbon materials to achieve a satisfactory efficiency and selectivity [7,12]. The proposed functionalization processes are targeted to improve the coordination properties of carbon species in order to capture more easily the pollutants in the aqueous solution. However, the molecules suggested for these purposes, for instance amine derivatives, can be very complex or intrinsically dangerous for both humans and environment [13].

In this scenario, membranes based on graphene oxide (GO) and related materials have attracted great interest from both academia and industry, even though GO structures are still debated [14–17], because of the complexity of the material and its non-stoichiometric composition [14,18–20].

Indeed, GO can be easily exfoliated in stable monolayer sheets and, owing to its polar functional groups, easily dispersed in water. Oxygenated groups are also responsible for the self-assembling properties of GO, which is able to arrange into membranes characterized by better mechanical properties compared to those shown by graphite-based materials [19]. Other properties that make GO and its derivatives promising candidates for membrane filtration processes are its high surface area and excellent water permeability, as well as its effective molecular sieve properties [21]. Moreover, GO offers realistic perspectives of production at industrial scale, since self-assembling membranes can be easily prepared by filtration of aqueous dispersions [14,22].

In the literature it has been proposed that reduced graphene oxide (rGO) can show improved filtration properties [19]. rGO can be easily obtained by reducing GO; the reduction may partially affect the ability of forming stable filter membranes, which is considered to rely on a macroscopic mechanical behavior [19,23]. Membrane formation derives from the abovementioned self-assembling capability of GO, which may be kept if a moderate and controlled reduction of its oxygen functional groups is carried out. As a matter of fact, the functional groups lying on GO basal planes are responsible for secondary bonds holding together the layers of GO itself [19]. A previous work has pointed out that cracks and uneven surfaces are obtained upon increasing the reduction time; in particular, the capability to form free-standing membranes is lost if 72 h of reduction are exceeded [19]. Indeed, the reduction has an effect on both pore size and interlayer distance, thus possibly increasing capture ability and/or selectivity toward different pollutants [24].

GO can be thermally reduced in an inert or reducing atmosphere at temperatures higher than 100 °C. The reduction takes place because of the progressive removal of the oxygenated functional groups; however, losses up to 30% can result in a detrimental loss of active material and in structural distortions [14]. Alternatively, chemical reduction with different reducing agents has been proposed. Hydrazine and its derivatives have been reported as reducing agents of choice [14]. However, hydrazine, in view of its many hazards for both humans and environment, poses major demands for more friendly and sustainable reagents. In this respect, L-ascorbic acid (L-AA) has been reported to show an effective capability in reducing GO [16].

With these premises, this paper proposes a simple process to obtain self-assembling rGO-based membrane filters starting from an aqueous dispersion of GO. Parameters optimization to obtain the membranes via vacuum filtration, as well as to achieve a proper reduction degree, are also assessed. Membranes morphological and micro-structural characterization is discussed in order to demonstrate their applicability as filters for metal-polluted wastewater and water softening [25,26].

Aqueous solutions with composition similar to real mining wastewater, containing Cu^{2+}, Fe^{3+}, Ni^{2+}, and Mn^{2+}, or close to drinkable water, containing Ca^{2+} and Mg^{2+}, have been used to prove the effectiveness of the proposed membranes. An attempt to understand ions capture mechanism and ions-sorbent interactions is also offered.

2. Materials and Methods

GO-based membranes were produced by vacuum filtration of a solution containing either GO or rGO, after reduction at different times (24, 48, and 72 h). L-ascorbic acid (L-AA) (Sigma Aldrich, Milan, Italy) was employed as reducing agent.

A 4 mg/mL commercial GO dispersion (Graphenea, San Sebastian, Spain) was used, consisting of monolayer GO flakes (<10 μm) dispersed in water at pH 2.2–2.5. The rGO solution was prepared according to [23] by diluting the commercial aqueous dispersion at a final GO concentration of 0.4 wt.%, after dehydrated L-AA was added in the ratio GO/L-AA = 1/10 (wt./wt.) [23]. The mixture was stirred at room temperature for 24, 48, or 72 h; these reduction times have already proved, in a previous work, to preserve both self-assembling properties and integrity of the membrane surface [23].

As reported in Figure 1, the suspension containing rGO was poured into a Gooch crucible sealed with a PVDF membrane filter (Millipore, Milan, Italy). Once the crucible was filled, vacuum was applied (water pump) until the formation of a self-standing membrane was completed. The membrane was then dried at 60 °C for 2 h. The same experimental route has also been applied to prepare GO membranes, without performing the reduction by L-AA.

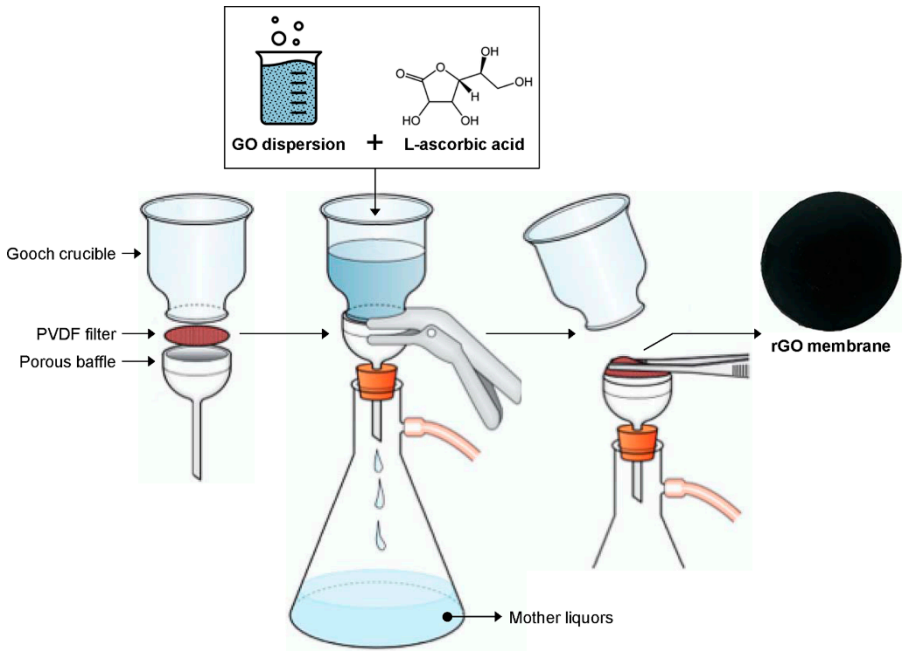

Figure 1. Schematic representation of the production process of reduced graphene oxide (rGO) membranes.

Morphology and structure of the membranes were analyzed by different techniques. FT-IR spectra were recorded with a FT-IR spectrometer Nicolet Nexus coupled with an IR-microscope ThermoElectron Continuμm (Thermo Fisher Scientific, Waltham, MA, USA). In order to reduce the possible structural changes of the membranes during the preparation of the specimen, a diamond anvil cell (DAC) accessory fitted to the 15Xreflective Cassegrain microscope (Thermo Fisher Scientific, Waltham, MA, USA) objective was used. A small portion of the membrane was placed into the DAC and analyzed in transmission mode accumulating 128 scans with a resolution of 4 cm^{-1}.

Raman spectra were recorded by a Jobin Yvon Labram HR800 Raman spectrometer (HORIBA Jobin Yvon, Kyoto, Japan) coupled with an Olympus BX41 microscope (Olympus Italia, Segrate, Italy) equipped with a 50X objective. The excitation line at 632.8 nm of a HeNe laser (Manufacture, City, State Abbr (if USA), Country) was applied. Spectra were recorded in a micro-Raman setup, placing the membrane directly under the microscope objective. The laser power was set at 50 μW to prevent heating effects or laser-induced graphitization/degradation of the samples. Spectra were recorded averaging four acquisitions each one of 30 s.

Both surface and cross-section of the produced membranes were analyzed by a scanning electron microscope (SEM) Zeiss EVO 50 EP (Zeiss, Jena, Germany) with a spectrometer OXFORD INCA energy 2000 (Oxford Instruments, Abingdon, UK). The samples were previously coated with a thin layer of gold in order to make their surfaces conductive. SEM was operated at an electron high tension (EHT) voltage of about 20 kV at high vacuum (around 10^{-5} torr).

X-ray diffraction (XRD) patterns of the membranes were collected in the range of 2–30° 2θ by using a Bruker D8 Advanced diffractometer (Bruker Italy, Milan, Italy), a monochromated Cu Kα radiation (λ = 0.154 nm), 0.02° 2θ of step scan and 1 s per step.

Thermogravimetric measurements were carried out up to 1000 °C by means of the EXSTAR 6000 TG/DTA 6300 (Seiko Instruments, Chiba, Japan), employing a nitrogen atmosphere (flow rate = 55 mL·min^{-1}) and a heating ramp of 10 °C·min^{-1}.

The filtration capability was tested by contacting a 4 mg rGO membrane with 50 mL of model solutions for 10 min, followed by vacuum filtration. Two different applications were considered: mine wastewater and drinkable water softening.

Mine wastewater composition, representing the concentrations detected in the final steps of common industrial purification processes prior to discharge [27], consists of Fe^{3+}, Mn^{2+}, Ni^{2+}, Cu^{2+} in molar ratios as depicted in Table 1.

Table 1. Composition of the mine wastewater model solution.

Ion	Concentration	
	[mg/L]	[mM]
Fe^{3+}	4	0.0716
Mn^{2+}	1	0.0182
Ni^{2+}	0.4	0.0068
Cu^{2+}	4	0.0063

Concerning water softening, Ca^{2+} and Mg^{2+} concentrations were set to reproduce the tap water concentration of our laboratory, i.e., 1 mmol/L for both ions.

As ions precursors, nitrates were selected for Ni^{2+} ($Ni(NO_3)_2 \cdot 6H_2O$) and Mg^{2+} ($Mg(NO_3)_2 \cdot 6H_2O$), while chlorides were used for Fe^{3+} ($FeCl_3 \cdot 6H_2O$), Ca^{2+} ($CaCl_2 \cdot 2H_2O$) and Mn^{2+} ($MnCl_2 \cdot 4H_2O$), all supplied by Sigma Aldrich.

Single ion and multi-ion solutions were analyzed, so as to evaluate the possible matrix effect or the mutual influence among ions when co-present in solution. Single ions concentrations were selected equal to the specific ion concentration in the corresponding multi-ion solution.

Metal analysis before and after the filtration step was performed by means of ICP-OES technique using a PerkinElmer OPTIMA 7000 DV spectrometer (Perkin Elmer Italia, Milan, Italy). The average of three measurements is reported, and the estimated measurement error is within 1%.

The capture efficiency was calculated by the difference between the initial ion concentration ($C_{0,i}$) in the starting solution and the residual one ($C_{f,i}$) according to Equation(1):

$$\eta_c(\%) = \frac{C_{0,i} - C_{f,i}}{C_{0,i}}.100 \quad (1)$$

3. Results and Discussion

3.1. Membranes Characterization

SEM images of both surface and cross-section of GO and rGO membranes, prepared with different reduction times, are reported in Figure 2.

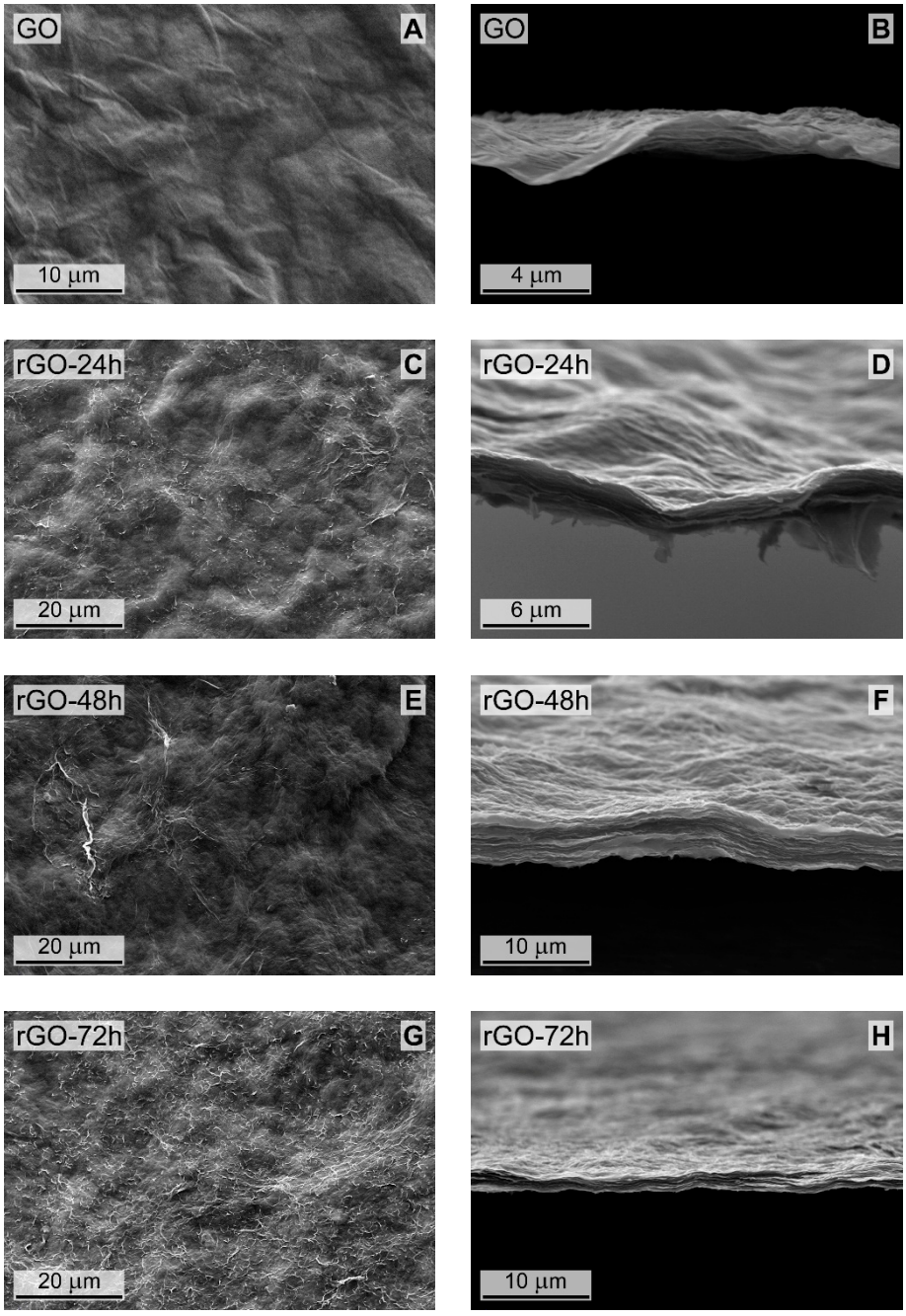

Figure 2. Surface (left) and cross-sectional (right) SEM images of (**A**,**B**) pristine GO; (**C**,**D**) rGO reduced for 24 h; (**E**,**F**) rGO reduced for 48 h; (**G**,**H**) rGO reduced for 72 h.

All rGO membranes exhibit an appreciable macroscopic roughness which increases with the reduction time. Moreover, the presence of several bright areas, that are less detectable on the pristine GO surface (Figure 2A), is also evident. Such a roughening effect, apparently related to reduction conditions, can be ascribed to a decrease of surface order upon increasing GO reduction time [23].

The analysis of the cross-sections shows that the slightly corrugated membranes are characterized by a macroscopic multilayer structure. The multilayer structure might originate from the production procedure, which implies the formation of the membrane by emptying, under vacuum, the funnel containing the GO or rGO dispersion. Therefore, the overall membrane thickness is the result of a continuous stacking of single layers. Apparently, the layers within a single membrane are characterized by similar thickness. No sharp differences were found among membranes obtained at different reduction times, and thicknesses in the range from 1.5 to 2.5 μm were measured for all the prepared membranes.

The XRD patterns of pristine GO and rGO membranes are plotted in Figure 3. Upon increasing the reduction time, one can observe a clear and progressive decrease of the intensity of the characteristic GO reflection around 11° 2θ [28,29]. A corresponding interlayer distance of 7.98 Å was calculated, more than two-fold that of graphite (d = 3.4 Å). The larger interlayer distance of GO has been reported to be due to the oxygen-containing functional groups of the basal plane and to water molecules intercalated between layers [23,28].

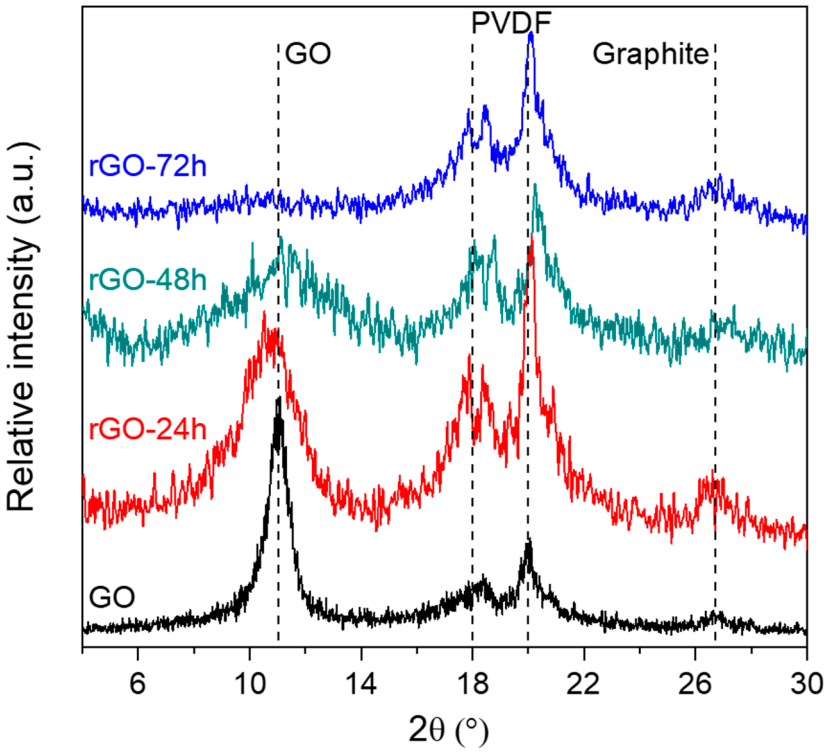

Figure 3. XRD patterns of GO and rGO membranes at different reduction times.

By increasing the reduction time, a progressive broadening of the GO reflection becomes evident; the calculated interlayer distance decreases from 7.98 to 3.3 Å for GO and rGO-48h, respectively, while for the sample reduced 72 h the 11° 2θ reflection is no longer detectable. After a prolonged reduction treatment, the material probably suffers an amorphization and a probable graphitization inception [30]. A progressive formation of graphite in the reduced samples is confirmed by the appearance of an additional reflection, even though wide and slightly pronounced, at 26.7° 2θ [31]. Broadness and intensity of such reflection may be related to graphite formation upon GO reduction. Indeed, in the presented samples graphite probably originates from graphene that, in turn, has been generated during the reduction of GO [32].

On the other hand, the diffractogram also exhibits the typical features of the PVDF membrane filter used in the funnel as support during GO-based membranes production, corresponding to the additional reflections at 18° and 20° 2θ. The PVDF membrane was kept while performing XRD measurements, in order to ensure a sufficient rigidity to rGO membranes and to prevent potential damages or corrugation during the analysis [23].

Therefore, it may be also possible to assign the reflection at 26.7° 2θ to the monoclinic α-phase of PVDF, resulting in an overlap with one of the graphites [33–35].

Figure 4 displays FT-IR (4A) and Raman (4B) spectra of the GO membrane compared with those of rGO membranes obtained after 24 and 72 h of reduction.

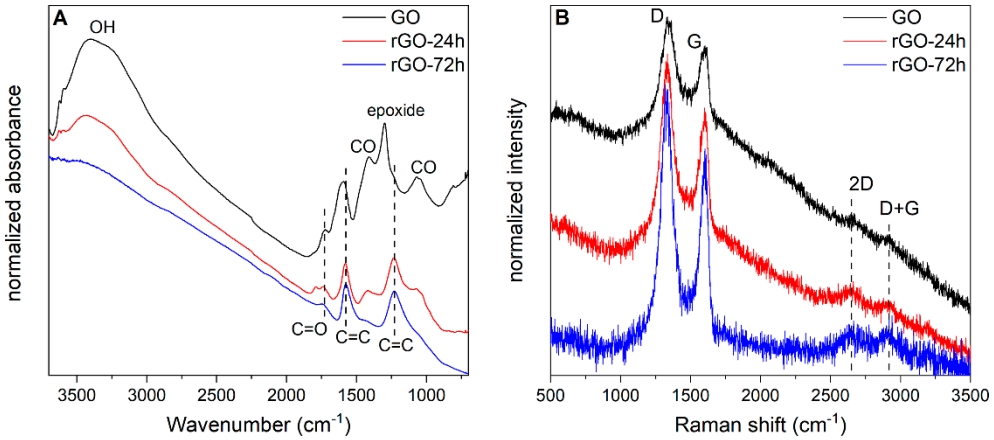

Figure 4. (**A**) FT-IR spectra and (**B**) Raman spectra (recorded with the laser line at 632.8 nm) of GO and rGO, reduced for 24 h and 72 h. The bands commented in the text are labelled; the spectra are stacked for the sake of clarity and are reported with normalized absorbance (FT-IR) or intensity (Raman).

In the FT-IR spectrum of the GO membrane (Figure 4A) it is possible to observe the spectroscopic features assigned to the presence of oxygenated functional groups which are characteristic of this class of materials [36]. In particular, we can identify: (i) in the 3500–3000 cm^{-1} region, the broad and strong absorption band assigned to the OH stretching vibrations; (ii) near 1750 cm^{-1}, the C=O stretching modes; (iii) the strong and structured band near 1600 cm^{-1}, assigned to the stretching vibrations of C=C bonds of GO layers; iv) in the 1400–900 cm^{-1} region, the intense absorptions due to the stretching and bending vibrations of CO groups; v) near 1300 cm^{-1}, the vibration of epoxy groups. Comparing the different spectra of the membranes, a decrease of the intensity of some bands is observed by increasing the time of reduction. In the spectrum of rGO-72h all the bands assigned to OH, COC, and epoxy functional groups are practically absent. The remaining ones located at 1730 cm^{-1} (C=O stretching), 1570 cm^{-1}, and 1250 cm^{-1} (C=C stretching vibrations which turn out to be IR enhanced by the polarizing effect of the residual C=O groups), suggest that during the process of reduction some extended but still structurally disordered graphene moieties grow inside the rGO layers. All Raman spectra (Figure 4B) show similar features, namely the G band near 1600 cm^{-1}, similar to the graphitic peak observed in graphene/graphite systems, assigned to the collective C=C stretching modes, and a D band near 1330 cm^{-1}, similar to the Disorder peak observable for chemically and or structurally disordered graphene layers [37]. Comparing the spectra of GO and rGO membranes, it is possible to observe, as a function of reduction time: (i) the decrease of the background, (ii) the sharpening of D and G bands, and (iii) the rise in intensity of the second order 2D and D + G bands. Considering the ratio I(D)/I(G), which describes the overall grade of disorder of graphene moieties, it is possible to calculate a value of 2.4 for the GO membrane and values of 2.1 and 2.0 for rGO-24h and rGO-72h membranes, respectively [36,38]. All these findings strongly suggest that graphene regions inside the rGO layers form and grow during the reduction process. The lower structural disorder and oxidation level observed for the rGO-72h sample with respect to the GO membrane can be also quantified by computing the average crystallites size as suggested in reference [15], resulting in an increase from 15.9 nm to 19.2 nm from GO to rGO-72h respectively.

The membranes were also characterized by thermogravimetric analysis; TG and DTG curves are reported in Figure 5A,B, respectively.

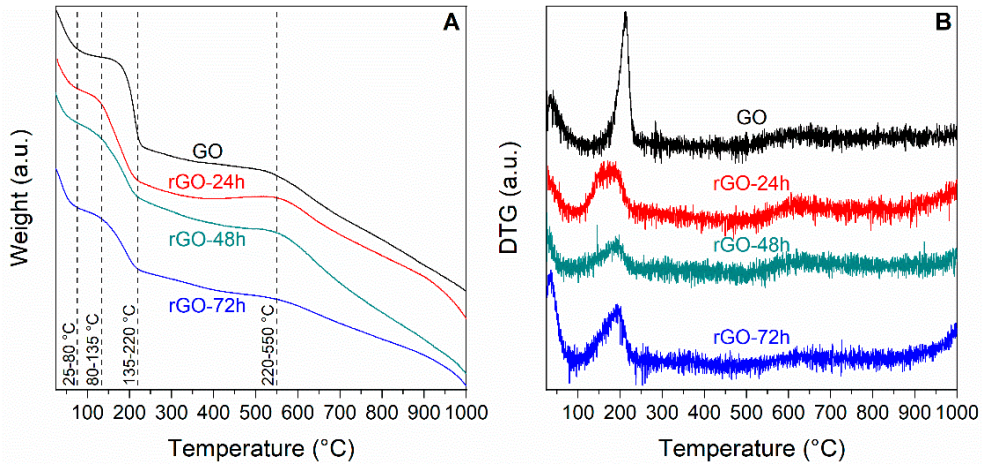

Figure 5. (**A**) TG and (**B**) DTG curves of pristine GO and rGO membranes reduced for different times.

A complex situation is evidenced in TG curves. Five fundamental weight losses, associated with different thermal phenomena, may be identified; for the sake of clarity, they are reported in Table 2 along with the corresponding temperature ranges and the hypothesized decomposition phenomena.

Table 2. Temperature ranges, weight losses, and decomposition phenomena of pristine GO and of rGO membranes reduced for different times.

T Range [°C]	Phenomenon	Weight Loss [%]			
		GO	rGO-24h	rGO-48h	rGO-72h
25–80	Evolution of physisorbed water	11.7	7.8	7.2	9.8
80–135	Evolution of intercalated water	3.0	3.3	4.0	4.3
135–220	Loss of weak oxygenated groups	25.0	24.0	18.1	14.5
220–550	Decomposition of oxygenated groups	7.2	5.0	10.2	8.6
550–1000	Breakdown of GO framework	34.0	34.4	40.4	24.9

The first thermal phenomenon, corresponding to the evolution of physically adsorbed water, takes place at temperatures lower than 80 °C and is common to all samples.

A second thermal phenomenon (Figure 5A, Table 2) occurs in the temperature range 80–135 °C; it accounts for weight losses of 3–4%, similar in all samples, which can be related to the evolution of water molecules intercalated in GO and rGO layers [39]. Such phenomenon can be identified in the DTG curves (Figure 5B) as the slight asymmetry on the left side of the stronger features detected at higher temperature. Its limited detection is mainly due to the small intensity of the phenomenon and to the strong overlapping of the two curves.

The third thermal phenomenon, occurring in the 135–220 °C range, is accompanied by marked weight losses; for instance, a loss of 25 wt.% was calculated for GO samples (Figure 5A, Table 2). However, the extent of the weight loss decreases by rising the reduction degree. Furthermore, the increasing of the reduction time induced a shift of the maxima of the DTG curves towards lower temperatures (Figure 5B). Temperature range, extent and symmetry of the DTG curve measured for GO (Figure 5B) suggest the decomposition of organic compounds. In particular, this phenomenon can be ascribed to the fast removal of oxygenated functional groups and consequent GO thermal reduction. Similar effects were observed also in rGO samples; however, the features were less intense

and broader, with maxima shifted to slightly lower temperatures. The associated weight losses progressively decrease on increasing the reduction time, from 25 wt.% of GO down to 14 wt.% of rGO-72h (Table 2). This phenomenon can be related to the presence of a lower number of oxygenated groups in the material, as expected upon reduction. Moreover, the broadening and the slight shift in the temperature of the maxima could suggest the presence of different thermal phenomena all occurring at very close temperatures, thus associated with oxygenated groups of different nature (i.e., carboxylate, anhydride or lactone ones [40]).

The thermal phenomenon taking place at higher temperatures (220–550 °C) corresponds to a limited weight loss (7–10 wt.%, Table 2), and it can be ascribed to the elimination of residual oxygenated functional groups, such as phenol and carbonyl ones, more strongly bonded to the GO backbone [41].

Finally, the progressive weight loss associated to the 550–1000 °C range corresponds to the breakdown of the GO framework [18].

3.2. Metal Capture Tests

As already reported, rGO-based materials, characterized by lower interlayer distance, showed remarkable performances in ions capture [19,24]. Indeed, if a lower amount of functional groups is present in reduced samples, layers are likely closer and this can definitely increase secondary bonds strength, which may imply a better effectiveness in ions capture due to electrostatic interactions. Therefore, rGO-72h sample was selected for filtration experiments in view of its close similarity with a graphitic material (i.e., interlayer distance about 3.3 Å), and because it retained the required self-assembling properties for membrane applications, despite the strong reduction.

Therefore, the following sections describe the preliminary results on the capture capability of rGO-72h membranes toward model solutions for water softening and for the adsorption of transition metal ions in mine wastewater. These tests, because of their limited number, are not supposed to be exhaustive, but they could allow lying the groundwork for the further development and production of filtration tools based on rGO.

For both applications, single ion and multi-ion solutions were considered and analyzed. Single ion solutions were employed first to enucleate the behavior of each ion toward sorbent interaction, then to compare the single ions behavior in a complex matrix. In real applications, indeed, wastewater containing a single component is not likely to be met.

3.2.1. Water Softening

For water softening experiments, the tap water of our laboratory was considered as reference; thus, model solutions containing either Ca^{2+} or Mg^{2+} ions were prepared first (1 mmol/L), followed by a bi-ion solution incorporating both Ca^{2+} and Mg^{2+} at the same concentration. In Figure 6, the results of filtration tests for both single ion and bi-ionic solutions are plotted in terms of ions capture efficiency.

Membrane capture in mono-ionic solutions evidenced an efficiency higher than 30% for both ions, but a slightly higher affinity toward Ca^{2+} can be inferred as well.

When the mixed solution of the ions, with comparable concentration, is analyzed, a decrease in capture efficiency can be found. However, the Ca^{2+} ions capture was only slightly lowered (−5%) while Mg capture was halved. These results suggest the presence of both a matrix effect and the already mentioned preferential capture toward Ca^{2+} ions. The slight decrease of Ca^{2+} capture efficiency can be explained with a competition for capture sites when also Mg^{2+} is present.

Considering these preliminary results, the use of rGO membranes can represent a valid alternative to other sorbent materials and would deserve further development.

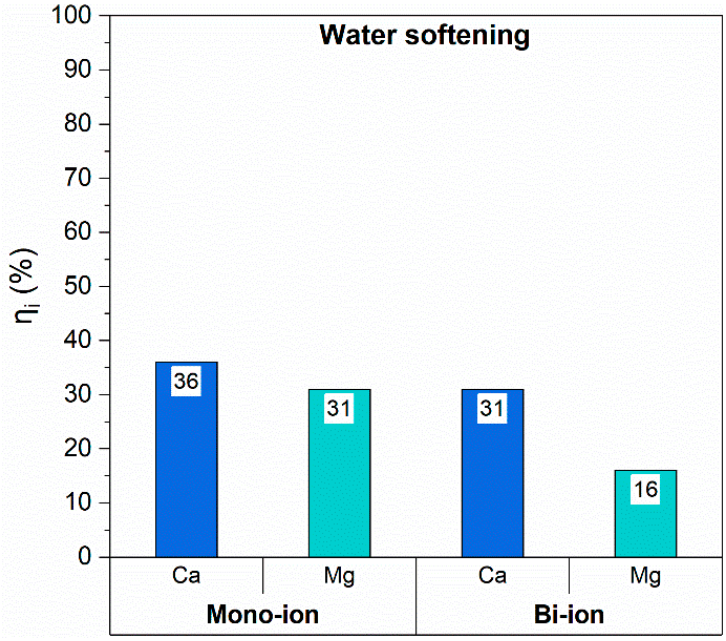

Figure 6. Ions capture efficiency for water softening tests.

3.2.2. Transition and Heavy Metals Capture in Mine Wastewater

Similarly to water softening applications, also mine wastewater was considered, and both mono-ionic solutions and multi-ion ones were analyzed. Results are plotted in Figure 7.

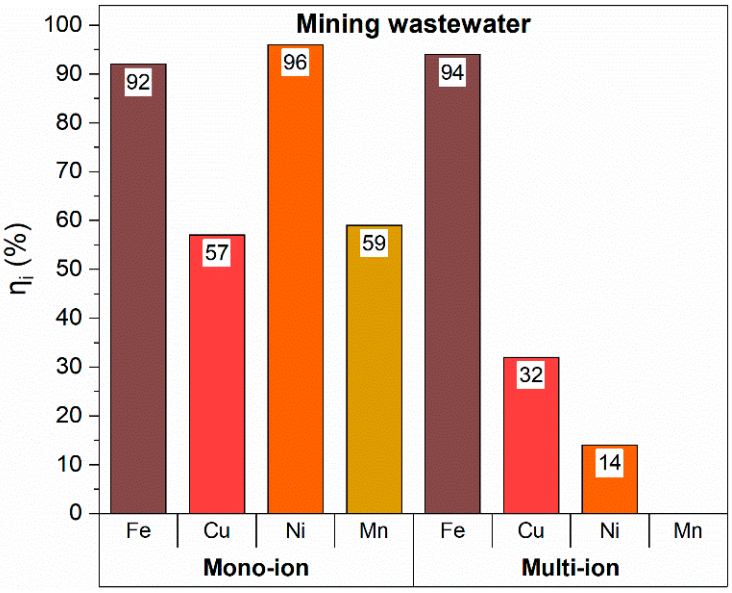

Figure 7. Ions capture efficiency for mine wastewater tests.

The sorbent material exhibited very high affinity toward all ions; indeed, capture efficiencies higher than 50% were calculated for all of them, with much larger affinity toward Fe^{3+} and Ni^{2+}, whose capture values even exceeded 90%.

The larger affinity for Fe^{3+} was preserved in multi-ion solutions too, where a capture efficiency of 94% was obtained. Conversely, a significant worsening affects the capture efficiency of the other components, particularly Ni^{2+} and Mn^{2+}. Indeed, Ni^{2+} capture decreased from 96% down to 14%, and Mn^{2+} was not captured at all. Once more, a strong matrix effect, i.e., a mutual influence among the ions when co-present, has to be considered.

However, sample sites saturation or site competition effects are not able to explain such a behavior in this case, because of Fe^{3+} constant capture. A possible explanation could be found in the mixed solution equilibria, where pH modification can occur in view of the co-presence of the different ions. Indeed, the pH value could shift ions equilibria toward more soluble species or aquo-complexes that are not able to interact with rGO capture sites. Therefore, pH values of both single- and multi-ion solutions were measured, and compared with the capture efficiency (ηi %). Results are reported in Table 3.

Table 3. pH of the mono- and multi-ion solutions and capture efficiency.

Ion	pH Mono	pH Multi	η_i % Mono	η_i % Multi
Fe^{3+}	3.8	3.7	92	94
Cu^{2+}	4.4		57	32
Ni^{2+}	5.0		96	14
Mn^{2+}	5.4		59	0

A pH effect on the multi-ion solution is quite clear. In the case of Fe^{3+} ions, for which the pH of the multi-ionic solution, i.e. 3.7, was the same of the mono-ionic one, i.e. 3.8, almost the same ion capture was maintained (96% and 94% for the mono- and the multi-ion solutions, respectively). The farther the pH of the multi-ionic solution is from that of the mono-ionic ones, the more marked is the decrease in the capture ability. Therefore, the retaining efficiency of Cu^{2+} ions is halved, that of Ni^{2+} ions is about 10% of the mono-ionic one, while no capture occurred for Mn^{2+} ions.

In order to better understand the pH effect, an analysis of the equilibria was performed on both mono-ionic and multi-ionic solutions with the Hydra-Medusa software (Version 16.1). This software is able to predict qualitatively the evolution of species in solutions as a function of pH, on the basis of thermodynamic data. The picture resulting from the analysis of the chemical equilibria of mono-ionic solutions is reported in Table 4. It can be noticed that, at the pH values of the operating conditions of the experiments (Table 3), all species are present in cationic or charged complex form, thus surely soluble. This is an important validation of the assumption that the ions are adsorbed on the membrane and not blocked as precipitated salts.

Table 4. pH ranges and corresponding species as computed by the Hydra-Medusa software.

Metal	pH Range		
	0–4	4–8	8–12
Fe	Fe^{2+} $FeOH^{2+}$ $FeCl^{2+}$ $Fe(OH)_2{}^{+}$	$Fe(OH)_{2.7}Cl_{0.3}$	Fe_2O_3
Cu	Cu^{2+} $CuCl^{+}$	$CuOH^{+}$ $Cu_2(OH)_2{}^{2+}$	CuO $Cu(OH)_3{}^{-}$ $Cu(OH)_4{}^{2-}$ $Cu(OH)_2$
Mn	Mn^{2+} $MnCl^{+}$	Mn^{2+} $MnCl^{+}$	$Mn_2(OH)_3{}^{+}$ $MnOH^{+}$ $Mn(OH)_2$
Ni	Ni^{2+}	$NiOH^{+}$	$Ni(OH)_2$ $Ni(OH)_3{}^{-}$

Regarding the comparison with the tri-ionic solution, the pH effect can be still inferred (all the ions are present in their cationic form); however, an additional phenomenon has to

be present to explain the preferential capture of Fe^{3+}. Accordingly, supposing the ions exert some electrostatic interaction with the residual functional groups of rGO, ions properties, such as dimensions and/or charges, have to be considered. The ionic radii (hydrated and non-hydrated) and their charge/radius ratio are compared in Table 5.

Table 5. Ionic radii and charge/radius ratio [42,43].

Ion	Ionic Radius [nm]	Hydrated Radius [nm]	Z^2/r [1/nm]
Fe^{3+}	0.065	0.480	140.63
Cu^{2+}	0.073	0.419	54.05
Ni^{2+}	0.069	0.404	57.14
Mn^{2+}	0.083	0.438	48.00

On the bases of data reported in Tables 3 and 5, the following considerations can be done. The permeation ability through a membrane can be generally explained on the basis of thermodynamic and physical characteristics of the involved species. Captured ions occupy surface sites and pore holes of the membrane, and the separation may be due to size exclusion or to the electrostatic characteristics of the ions in the aqueous phase [42,44]. The oxygen functional groups of GO play a role as well in determining the interlayer spacing and the interaction with cations [45]. At the same time, water or ions could insert themselves into the graphene layers and increase the interlayer spacing. In dry conditions, the GO membrane has a d-spacing of about 8 Å, while in liquid media this value may reach 14 Å.

On the other hand, after reduction rGO exhibits defects that facilitate the movement of water molecules and, at the same time, reduce the interlayer distance toward the graphite value, i.e., 3.4 Å. This narrow spacing allows both charge selectivity and sieving depending on the type and diameter of hydrated ions [46,47].

At a first glance, the size exclusion mechanism may be considered more plausible because the reduction process causes narrower d-spacing between sheets and lower electrostatic interactions, following the loss of functional groups. Therefore, if the diameter of hydrated ions is larger than rGO channels, the ions are retained by the membrane because of steric hindrance.

However, another possible explanation, laying on electrostatic considerations, can be given observing the Z^2/r ratio as well as the flexibility of the hydration shell. The Z^2/r ratio is correlated to the hydration potential, which denotes the attraction between an ion and water molecules. For larger ions, the charge is more dispersed, therefore the hydration shell is held with a weaker electric field. On the contrary, if the hydration shell is held strongly, cations can be blocked in the hydrophilic regions of the membrane. In general, the hydrated shell of small cations remains unchanged and the water molecules around them are at a fixed distance even if they are constantly exchanged with bulk ones [42,47].

Water flows through the hydrophobic non-oxidized sp^2 regions formed between the contiguous nanosheets rather than in oxidized regions. However, the available hydrophobic regions in these membranes are insufficient to form well-defined nanochannels [44].

Concerning the experiments on water softening of this work, the higher selectivity for Ca^{2+} might be due to steric hindrance, its radius being larger than that of Mg^{2+}. On the contrary, as far as model solutions of mining wastewater are concerned, the higher capture efficiency for Fe^{3+} ions might be explained focusing on ions size in the hydrated form and on the ionic charge. Indeed, Fe^{3+} has a hydrated ionic radius larger than the other ones and a greater charge, so it can interact more strongly with rGO surface functional groups. Focusing on Mn^{2+}, the charge is very similar to the one of Cu^{2+} and Ni^{2+}, but the hydrated radius and the Z^2/r ratio are similar or greater. After the contacting step with the multi-ion solution, it greatly permeates through the membrane. This unexpected behavior was also reported in other studies [48], which proved how adsorption may be sometimes influenced by the specific kind of coordination and in particular by the related geometry, square-planar for Cu^{2+} [49] while trigonal-bipyramidal for Mn^{2+} [50]. The difference in coordination results in a smaller average distance between Cu^{2+} and carboxylate groups

and a higher interaction energy; on the other hand, the Mn^{2+} conformation is less stable and this may lead to a lower capability to be adsorbed by the filter [48]. Therefore, when differently charged ions are present in the solution to be treated, it seems that an electrostatic mechanism is prevailing and, regarding this work, this may be the reason why iron has been captured more effectively compared to other ions.

Table 6 shows the effectiveness of the rGO-72h membrane in terms of adsorption capacity (in mg of captured metal over the sorbent mass).

Table 6. Sorption capacity of the rGO-72 membrane for metal ions removal in mono- and multi-ion solutions.

Ion	Adsorption Capacity (mono-ion) [mg/g]	Adsorption Capacity (multi-ion) [mg/g]
Fe^{3+}	38.4	37.0
Cu^{2+}	27.4	14.9
Ni^{2+}	16.0	4.2
Mn^{2+}	12.2	-

A precise and explicit comparison is not easy with efficiency values reported in the literature for other carbon-based materials because of the great variety of operating conditions and treated polluted solutions, but an appreciable agreement has been found. Indeed, various studies have been conducted about the use of carbon nanotubes [51], biochar fabricated from biomasses [52], activated carbons [53] in several processes intended to remove heavy metals such as Fe, Cu, Mn, Ni, Pb, Cd, Hg, Cr, Zn, Co with efficiencies variable in the range 1–70 mg/g, but such values are strongly influenced by the specific operating conditions, techniques, plants, and ions concentrations. GO-based composites, mainly used as powders interacting for several hours with polluted solutions to be treated, have also been developed to remove and/or recover toxic or precious metals such as Pb, Cr, Fe, Cd, Zn, Mn, Cu, Au [54–57]. Capacities higher than 100 mg/g have been obtained for Cu removal [55,56] while values around 20 mg/g have been calculated upon treating Fe- and Mn-containing solutions [58].

4. Conclusions

Self-assembling membranes based on graphene oxide (GO) have been developed aiming to be used as filter in the treatment of wastewater containing metal ions. A facile, inexpensive, and eco-friendly chemical reduction route was employed exploiting L-ascorbic acid as the reducing agent. Among differently reduced membranes, the one reduced for 72 h, showing significant amorphization and graphitization while keeping the self-assembling behavior, was selected for preliminary filtration tests. Indeed, it was assumed that a lower interlayer distance compared to GO or less reduced rGO membranes can effectively influence the capability in ions capture.

Model solutions for both water softening applications and transition metal ions from the mining industry have been treated. Single- and multi-ion solutions have been considered in order to assess selectivity toward different species and to account for possible adsorption sites competition and matrix effects.

Concerning water softening experiments, rGO filters proved to be more selective toward Ca^{2+} ions, likely because of their higher ionic radius compared to Mg^{2+}. On the contrary, as far as the transition metal ions solution is concerned, all the species showed a satisfying affinity (capture efficiencies between 57% and 96%) with rGO in single-ion tests, whereas a high capture efficiency (>90%) was kept for Fe^{3+} only in the more realistic multi-ion experiments. This may be ascribed to electrostatic reasons since Fe^{3+} presents a higher charge that can enhance the interaction with the filter adsorption sites.

The preliminary results of this work seem to be promising in terms of the feasibility of the use of rGO as filter in wastewater treatment and of its selectivity toward specific

ions, as well as to boost further studies investigating several wastewater concentrations and possible recovery of the adsorbed species.

Author Contributions: Conceptualization, C.C., S.L., G.D.; methodology, C.C., M.B., S.L.; investigation, S.L., L.B., A.B.P.; data curation: C.C., G.R.; writing—original draft preparation, S.L., A.B.P., L.B.; writing—review and editing, C.C., E.F., G.D., visualization, S.L., M.B., P.G.S.; supervision, C.C., E.F., G.D. All authors have read and agreed to the published version of the manuscript.

Funding: This research received no external funding.

Institutional Review Board Statement: Not applicable.

Informed Consent Statement: Not applicable.

Data Availability Statement: The data presented in this study are available on request from the corresponding author.

Acknowledgments: The authors gratefully acknowledge Eng. Francesca Chignoli, Eng. Giuseppe D'Andrea (Politecnico di Milano) and Buddhika Rathnayake (University of Oulu) for their help in performing experiments and modeling equilibrium phenomena.

Conflicts of Interest: The authors declare no conflict of interest.

References

1. Qu, X.; Alvarez, P.J.J.; Li, Q. Applications of nanotechnology in water and wastewater treatment. *Water Res.* **2013**. [CrossRef]
2. World Health Organization. *WHO and UNICEF Progress on Drinking Water, Sanitation and Hygiene: 2017 Update and SDG Baseline*; World Health Organization: Geneva, Switzerland, 2017.
3. Chen, Y.; Chen, L.; Bai, H.; Li, L. Graphene oxide-chitosan composite hydrogels as broad-spectrum adsorbents for water purification. *J. Mater. Chem. A* **2013**. [CrossRef]
4. Letterman, R. *Water Quality and Treatment, a Handbook of Community Water Supplies*, 5th ed.; American Water Works Association, McGraw-Hill Inc.: New York, NY, USA, 1999.
5. Iannicelli-Zubiani, E.M.; Cristiani, C.; Dotelli, G.; Gallo Stampino, P. Recovery of valuable metals from electronic scraps by clays and organo-clays: Study on bi-ionic model solutions. *Waste Manag.* **2017**. [CrossRef] [PubMed]
6. Iannicelli-Zubiani, E.M.; Cristiani, C.; Dotelli, G.; Gallo Stampino, P.; Pelosato, R.; Mesto, E.; Schingaro, E.; Lacalamita, M. Use of natural clays as sorbent materials for rare earth ions: Materials characterization and set up of the operative parameters. *Waste Manag.* **2015**. [CrossRef] [PubMed]
7. Saleem, H.; Zaidi, S.J. Developments in the Application of Nanomaterials for Water Treatment and Their Impact on the Environment. *Nanomaterials* **2020**, *10*, 1764. [CrossRef] [PubMed]
8. Han, H.; Rafiq, M.K.; Zhou, T.; Xu, R.; Mašek, O.; Li, X. A critical review of clay-based composites with enhanced adsorption performance for metal and organic pollutants. *J. Hazard. Mater.* **2019**. [CrossRef]
9. Santhosh, C.; Velmurugan, V.; Jacob, G.; Jeong, S.K.; Grace, A.N.; Bhatnagar, A. Role of nanomaterials in water treatment applications: A review. *Chem. Eng. J.* **2016**, *306*, 1116–1137. [CrossRef]
10. Alnoor, O.; Laoui, T.; Ibrahim, A.; Kafiah, F.; Nadhreen, G.; Akhtar, S.; Khan, Z. Graphene oxide-based membranes for water purification applications: Effect of plasma treatment on the adhesion and stability of the synthesized membranes. *Membranes (Basel)* **2020**, *10*, 292. [CrossRef]
11. Zouzelka, R.; Remzova, M.; Plsek, J.; Brabec, L.; Rathousky, J. Immobilized rGO/TiO2 photocatalyst for decontamination of water. *Catalysts* **2019**, *9*, 708. [CrossRef]
12. Jawed, A.; Saxena, V.; Pandey, L.M. Engineered nanomaterials and their surface functionalization for the removal of heavy metals: A review. *J. Water Process Eng.* **2020**, *33*, 101009. [CrossRef]
13. Iannicelli-Zubiani, E.M.; Gallo Stampino, P.; Cristiani, C.; Dotelli, G. Enhanced lanthanum adsorption by amine modified activated carbon. *Chem. Eng. J.* **2018**. [CrossRef]
14. Khan, Z.U.; Kausar, A.; Ullah, H.; Badshah, A.; Khan, W.U. A review of graphene oxide, graphene buckypaper, and polymer/graphene composites: Properties and fabrication techniques. *J. Plast. Film Sheeting* **2016**, *32*, 336–379. [CrossRef]
15. Krishnamoorthy, K.; Veerapandian, M.; Yun, K.; Kim, S.J. The chemical and structural analysis of graphene oxide with different degrees of oxidation. *Carbon N. Y.* **2013**. [CrossRef]
16. Zhu, Y.; Murali, S.; Cai, W.; Li, X.; Suk, J.W.; Potts, J.R.; Ruoff, R.S. Graphene and graphene oxide: Synthesis, properties, and applications. *Adv. Mater.* **2010**. [CrossRef]
17. Stankovich, S.; Dikin, D.A.; Piner, R.D.; Kohlhaas, K.A.; Kleinhammes, A.; Jia, Y.; Wu, Y.; Nguyen, S.B.T.; Ruoff, R.S. Synthesis of graphene-based nanosheets via chemical reduction of exfoliated graphite oxide. *Carbon N. Y.* **2007**. [CrossRef]
18. Basso Peressut, A.; Latorrata, S.; Gallo Stampino, P.; Dotelli, G. Development of self-assembling sulfonated graphene oxide membranes as a potential proton conductor. *Mater. Chem. Phys.* **2021**, *257*, 123768. [CrossRef]

19. Chen, C.; Yang, Q.H.; Yang, Y.; Lv, W.; Wen, Y.; Hou, P.X.; Wang, M.; Cheng, H.M. Self-assembled free-standing graphite oxide membrane. *Adv. Mater.* **2009**. [CrossRef]
20. Eda, G.; Chhowalla, M. Chemically Derived Graphene Oxide: Towards Large-Area Thin-Film Electronics and Optoelectronics. *Adv. Mater.* **2010**, *22*, 2392–2415. [CrossRef]
21. Han, Y.; Xu, Z.; Gao, C. Ultrathin graphene nanofiltration membrane for water purification. *Adv. Funct. Mater.* **2013**. [CrossRef]
22. Guoxiu, W.; Juan, Y.; Jinsoo, P.; Xinglong, G.; Bei, W.; Hao, L.; Jane, Y. Facile synthesis and characterization of graphene nanosheets. *J. Phys. Chem. C* **2008**. [CrossRef]
23. Migliavacca, A.; Latorrata, S.; Gallo Stampino, P.; Dotelli, G. Preparation and characterization of graphene oxide based membranes as possible Gas Diffusion Layers for PEM fuel cells with enhanced surface homogeneity. *Mater. Today Proc.* **2017**, *4*, 11594–11607. [CrossRef]
24. Mi, B. Graphene Oxide Membranes for Ionic and Molecular Sieving. *Science* **2014**, *343*, 740–742. [CrossRef] [PubMed]
25. Tuan, T.N.; Chung, S.; Lee, J.K.; Lee, J. Improvement of water softening efficiency in capacitive deionization by ultra purification process of reduced graphene oxide. *Curr. Appl. Phys.* **2015**. [CrossRef]
26. World Health Organization. *WHO Guidelines for Drinking-water Quality*; World Health Organization: Geneva, Switzerland, 2008.
27. D'Andrea, G. *Report: Private Communication between University Groups (Politecnico di Milano and Oulu University) and Industry*, 2019.
28. Jiao, X.; Qiu, Y.; Zhang, L.; Zhang, X. Comparison of the characteristic properties of reduced graphene oxides synthesized from natural graphites with different graphitization degrees. *RSC Adv.* **2017**. [CrossRef]
29. Wei, L.; Mao, Y. Enhanced hydrogen storage performance of reduced graphene oxide hybrids with nickel or its metallic mixtures based on spillover mechanism. *Int. J. Hydrog. Energy* **2016**. [CrossRef]
30. Park, S.; An, J.; Potts, J.R.; Velamakanni, A.; Murali, S.; Ruoff, R.S. Hydrazine-reduction of graphite- and graphene oxide. *Carbon N. Y.* **2011**. [CrossRef]
31. Moon, I.K.; Lee, J.; Ruoff, R.S.; Lee, H. Reduced graphene oxide by chemical graphitization. *Nat. Commun.* **2010**. [CrossRef]
32. Ding, J.; Yan, W.; Xie, W.; Sun, S.; Bao, J.; Gao, C. Highly efficient photocatalytic hydrogen evolution of graphene/YInO 3 nanocomposites under visible light irradiation. *Nanoscale* **2014**. [CrossRef]
33. Cai, X.; Lei, T.; Sun, D.; Lin, L. A critical analysis of the α, β and γ phases in poly(vinylidene fluoride) using FTIR. *RSC Adv.* **2017**. [CrossRef]
34. Amouamouha, M.; Gholikandi, G.B. Characterization and antibiofouling performance investigation of hydrophobic silver nanocomposite membranes: A comparative study. *Membranes (Basel)* **2017**, *7*, 64. [CrossRef]
35. Van Goethem, C.; Magboo, M.M.; Mertens, M.; Thijs, M.; Koeckelberghs, G.; Vankelecom, I.F.J. A scalable crosslinking method for PVDF-based nanofiltration membranes for use under extreme pH conditions. *J. Memb. Sci.* **2020**. [CrossRef]
36. Acik, M.; Lee, G.; Mattevi, C.; Chhowalla, M.; Cho, K.; Chabal, Y.J. Unusual infrared-absorption mechanism in thermally reduced graphene oxide. *Nat. Mater.* **2010**, *9*, 840–845. [CrossRef]
37. Ferrari, A.; Robertson, J. Interpretation of Raman spectra of disordered and amorphous carbon. *Phys. Rev. B Condens. Matter Mater. Phys.* **2000**. [CrossRef]
38. Tuinstra, F.; Koenig, J.L. Raman spectrum of graphite. *J. Chem. Phys.* **1970**. [CrossRef]
39. Bose, S.; Drzal, L.T. Role of thickness and intercalated water in the facile reduction of graphene oxide employing camera flash. *Nanotechnology* **2014**. [CrossRef] [PubMed]
40. Huang, N.M.; Chang, B.Y.S. Facile hydrothermal preparation of titanium dioxide decorated reduced graphene oxide nanocomposite. *Int. J. Nanomed.* **2012**, *7*, 3379. [CrossRef] [PubMed]
41. Sengupta, I.; Chakraborty, S.; Talukdar, M.; Pal, S.K.; Chakraborty, S. Thermal reduction of graphene oxide: How temperature influences purity. *J. Mater. Res.* **2018**. [CrossRef]
42. Tansel, B. Significance of thermodynamic and physical characteristics on permeation of ions during membrane separation: Hydrated radius, hydration free energy and viscous effects. *Sep. Purif. Technol.* **2012**. [CrossRef]
43. VanLoon, G.W.; Duffy, S.J. Environmental chemistry: A global perspective. *Choice Rev. Online* **2011**, *48*. [CrossRef]
44. Rajesh, S.; Bose, A.B. Development of Graphene Oxide Framework Membranes via the "from" and "to" Cross-Linking Approach for Ion-Selective Separations. *ACS Appl. Mater. Interfaces* **2019**. [CrossRef] [PubMed]
45. Park, S.; Lee, K.S.; Bozoklu, G.; Cai, W.; Nguyen, S.B.T.; Ruoff, R.S. Graphene oxide papers modified by divalent ions Enhancing mechanical properties via chemical cross-linking. *ACS Nano* **2008**. [CrossRef] [PubMed]
46. Narayan, P.S.; Teradal, N.L.; Jaldappagari, S.; Satpati, A.K. Eco-friendly reduced graphene oxide for the determination of mycophenolate mofetil in pharmaceutical formulations. *J. Pharm. Anal.* **2018**. [CrossRef] [PubMed]
47. Kim, J.; Lee, S.E.; Seo, S.; Woo, J.Y.; Han, C.S. Near-complete blocking of multivalent anions in graphene oxide membranes with tunable interlayer spacing from 3.7 to 8.0 angstrom. *J. Membr. Sci.* **2019**. [CrossRef]
48. Sun, P.; Zhu, M.; Wang, K.; Zhong, M.; Wei, J.; Wu, D.; Xu, Z.; Zhu, H. Selective ion penetration of graphene oxide membranes. *ACS Nano* **2013**. [CrossRef]
49. Rulisek, L.; Havlas, Z. Theoretical studies of metal ion selectivity. 1. DFT calculations of interaction energies of amino acid side chains with selected transition metal ions (Co2+, Ni2+, Cu2+, Zn2+, Cd2+, and Hg2+). *J. Am. Chem. Soc.* **2000**. [CrossRef]
50. Marino, T.; Toscano, M.; Russo, N.; Grand, A. Structural and electronic characterization of the complexes obtained by the interaction between bare and hydrated first-row transition-metal ions (Mn 2+, Fe2+, Co2+, Ni2+, Cu2+, Zn 2+) and glycine. *J. Phys. Chem. B* **2006**. [CrossRef]

51. Ozcan, S.G.; Satiroglu, N.; Soylak, M. Column solid phase extraction of iron(III), copper(II), manganese(II) and lead(II) ions food and water samples on multi-walled carbon nanotubes. *Food Chem. Toxicol.* **2010**. [CrossRef]
52. Shakoor, M.B.; Ali, S.; Rizwan, M.; Abbas, F.; Bibi, I.; Riaz, M.; Khalil, U.; Niazi, N.K.; Rinklebe, J. A review of biochar-based sorbents for separation of heavy metals from water. *Int. J. Phytoremediation* **2020**, *22*, 111–126. [CrossRef]
53. Hashemi, B.; Rezania, S. Carbon-based sorbents and their nanocomposites for the enrichment of heavy metal ions: A review. *Microchim. Acta* **2019**, *186*, 578. [CrossRef]
54. Duru, İ.; Ege, D.; Kamali, A.R. Graphene oxides for removal of heavy and precious metals from wastewater. *J. Mater. Sci.* **2016**, *51*, 6097–6116. [CrossRef]
55. Wu, W.; Yang, Y.; Zhou, H.; Ye, T.; Huang, Z.; Liu, R.; Kuang, Y. Highly efficient removal of Cu(II) from aqueous solution by using graphene oxide. *Water Air Soil Pollut.* **2013**. [CrossRef]
56. Sitko, R.; Turek, E.; Zawisza, B.; Malicka, E.; Talik, E.; Heimann, J.; Gagor, A.; Feist, B.; Wrzalik, R. Adsorption of divalent metal ions from aqueous solutions using graphene oxide. *Dalton Trans.* **2013**. [CrossRef]
57. Manousi, N.; Rosenberg, E.; Deliyanni, E.A.; Zachariadis, G.A. Sample preparation using graphene-oxide-derived nanomaterials for the extraction of metals. *Molecules* **2020**, *25*, 2411. [CrossRef] [PubMed]
58. Pourjavid, M.R.; Sehat, A.A.; Arabieh, M.; Yousefi, S.R.; Hosseini, M.H.; Rezaee, M. Column solid phase extraction and flame atomic absorption spectrometric determination of manganese(II) and iron(III) ions in water, food and biological samples using 3-(1-methyl-1H-pyrrol-2-yl)-1H-pyrazole-5-carboxylic acid on synthesized graphene oxide. *Mater. Sci. Eng. C* **2014**. [CrossRef] [PubMed]